ChemComm

Sub-bandgap trap sites for high-density photochemical electron storage in colloidal $SrTiO_3$ nanocrystals

Journal:	*ChemComm*
Manuscript ID	CC-COM-08-2022-004328.R1
Article Type:	Communication

COMMUNICATION

Sub-bandgap trap sites for high-density photochemical electron storage in colloidal $SrTiO_3$ nanocrystals

Muhammad Abdullah, Ruby J. Nelson, and Kevin R. Kittilstved*

Received 00th January 20xx,
Accepted 00th January 20xx

DOI: 10.1039/x0xx00000x

We report facile and reversible electron storage in colloidal $SrTiO_3$ nanocrystals using photochemical and redox titration methods. A very high electron storage capacity (~180 e^- per 7 nm nanocrystal) is achieved which we attribute to the localized nature of added electrons at sub-bandgap trap sites in these colloidal $SrTiO_3$ nanocrystals. The rate of electron accumulation is also found to be much faster with ethylene glycol as the sacrificial reductant compared to ethanol. This work provides key insight and establishes a kinetic bottleneck in the charge trapping processes.

The global energy crisis and growing demand for more sustainable energy development are some of the grand challenges in today's world.[1] To overcome the intermittent availability of energy from renewable resources such as sunlight and wind, unifying energy conversion and storage in a single unit is one of the promising directions.[2] In this context, colloidal nanocrystals (NCs) are emerging as extremely versatile materials for light-driven multi-charge accumulation in a single system.[3,4] This light-induced charge storage involves capturing the photogenerated holes with sacrificial reductant which results in the addition of multiple electrons to the NCs. This process is typically known as photodoping. The opportunity to access multiple electrons implies an increase in carrier density which directly translate into their efficient application in batteries, capacitors, and multielectron redox catalysis.[5-7] However, only a limited number of electrons have been introduced with photodoping owing to various competing processes which have not been fully understood.[8] Some of us have recently reported a remarkable increase in the number of electrons stored in colloidal ZnO NCs through Fe^{3+} doping.[9] These ZnO NCs possess a set of redox-active $Fe^{3+/2+}$ energy levels situated below the conduction band that allows a large number of additional electron accumulation. The maximum number of photodoped electrons that can be stored in nominally pure ZnO NCs scales with the NC volume, $\langle N_{max} \rangle$ = 1.4(4) × 10^{20} cm^{-3}.[10] The introduction of Fe^{3+} dopants enabled additional electrons to be stored within the NCs that scale linearly with the dopant concentration. In contrast to Al^{3+} doping, which also increases N_{max}, the redox-active Fe^{3+} dopant provides an effective strategy to increase both the number of electrons that can be stored *and* transferred in colloidal semiconductor NCs.

We reported the photodoping of $SrTiO_3$-based NCs and found similar observations to the work on TiO_2 nanoparticles by Mayer et al.[11] Specifically, the excess electrons introduced by photodoping created Ti^{3+} traps through a "self-trapping" process involving the relaxation of a conduction band electron comprised primarily of empty Ti^{4+} 3d orbitals.[12] This is in contrast to ZnO NCs where the excess electrons remain delocalized within the conduction band that is susceptible to quantum confinement effects.[13] The degree of localization of the resulting Ti^{3+} defect has been the subject of intense experimental and theoretical study in bulk TiO_2 and $SrTiO_3$ semiconductors.[14] Subtle differences caused by variation in the electronic and physical structure of TiO_2 and $SrTiO_3$ may lead to significant effects on the photodoping processes. Although TiO_2 and $SrTiO_3$ have similar band gap energies, the presence of the A-site cation (Sr^{2+} or Ba^{2+}) has been reported to raise the energies of the valence and conduction bands of $ATiO_3$ by ~0.4 eV compared to TiO_2-anatase.[15] The corresponding Ti^{3+} trap depth could therefore be significantly deeper in $SrTiO_3$ NCs leading to more localized defect wavefunction and possibly higher charge storage capacity.

In the current study, we quantified the photochemical electron accumulation process in colloidal $SrTiO_3$ nanocubes with average edge lengths of *ca.* 7 nm (see electronic supplementary information (ESI) S1). The synthesis and characterization of colloidal $SrTiO_3$ NCs were completed following our recent work.[16] A detailed procedure for introducing excess electrons *via* photodoping is described in the ESI. Briefly, an anaerobic suspension of $SrTiO_3$ NCs in hexanes was irradiated with unfiltered light from a 75 W Xe arc-lamp to generate a conduction band electron and valence band hole. The valence band hole is filled by a sacrificial reductant leaving an extra electron in the NCs. Fig. 1 shows the electronic absorption spectra of anaerobic colloidal $SrTiO_3$ NCs in hexanes

Department of Chemistry, University of Massachusetts Amherst, 710 N Pleasant St, Amherst, MA 01003, USA. E-mail: kittilstved@chem.umass.edu
Electronic Supplementary Information (ESI) available: Additional EPR, NMR, and absorption spectra and tables are provided. Detailed pictures of the air-tight cuvette and syringe and calculations to quantify the number of electrons per nanocrystal are also provided. See DOI: 10.1039/x0xx00000x

with ethanol as the hole scavenger collected as a function of photoirradiation time up to 600 min. The electronic absorption spectrum of the as-prepared NCs is dominated by band gap transition above ~3.25 eV consistent with single-crystal $SrTiO_3$.[17] Photodoping changes the physical appearance of the sample from colorless to dark blue that is caused by the growth of a new broad absorption feature that is centered at ~1.5 eV and extends throughout the entire visible region. This electronic transition in the near-IR is consistent with photoirradiated TiO_2 and $SrTiO_3$ colloids in the presence of hole scavengers.[11,12,18-20] Excess electrons in the conduction band electron (e_{CB}^-) of semiconductors are typically observed spectroscopically by significant blue shifts in the band-edge energy from the Moss-Burstein effect and a characteristic localized surface plasmon resonance (LSPR) in the mid-IR region.[21,22] The lack of both the absorption in the mid-IR region and Moss-Burstein effect in our study suggests that photochemically-added electrons in $SrTiO_3$ NCs are not delocalized in the conduction band.

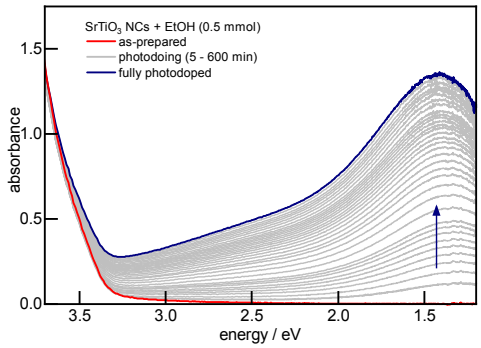

Fig. 1 Electronic absorption spectra of $SrTiO_3$ NCs as a function of photodoping time in the presence of ethanol as a sacrificial reductant (~1000 EtOH/NC). Color photographs of samples taken before and after photodoping are shown on the right side of the figure.

Free carriers in the conduction band of TiO_2 NCs can be forced to localize at Ti^{3+} shallow traps at cryogenic temperatures but are thermally detrapped at room temperature. These electrons can be observed by electron paramagnetic resonance (EPR) spectroscopy only below ~100 K when they are trapped at Ti^{3+} sites. The room-temperature EPR spectrum of photodoped $SrTiO_3$ NCs however shows a broad isotropic signal at g = 1.94 which suggests that added electrons are localized even at ambient temperature (see Fig. S2). This observation of an isotropic signal is consistent with Ti^{3+} sitting at the octahedral B-site and has been observed previously in photodoped Cr- and Fe-doped $SrTiO_3$ NCs.[12,20] Room-temperature EPR signals from titanium(III)-related defects have also been previously reported in reduced Ti(IV)-oxo clusters[23] and other molecular Ti^{3+} species.[24,25] We propose that the metal-to-metal charge transition from these localized Ti^{3+} sites to the conduction band (Ti^{4+}) gives rise to the broad absorption and blue coloration of the photodoped $SrTiO_3$ NCs. The origin of a similar blue transition has also been assigned in reduced rutile TiO_2 as a $Ti^{3+}Ti^{4+}$ pair intervalence charge transfer (IVCT) transition.[26] Assignment of the near-IR transition to the spin-allowed $^2T_2 \rightarrow {}^2E$ transition of a pseudo-octahedral Ti^{3+} defect site was also ruled out due to intensity considerations.

To gain insight into the kinetics of electron accumulation, we further plotted the changes in absorbance at 1.5 eV against time. The data displayed in Fig. 2 shows a rapid growth of absorption at the initial stages where one-half of the maximum photodoping is achieved within the first 100 min for the sample being photodoped in the presence of ~1000 equivalents of EtOH. We speculate that the photophysical origin of this rapid increase could be underlying competing processes. The successful electron addition is fundamentally governed by the reactivity of photogenerated holes towards (a) sacrificial reductant and (b) multicarrier recombination processes as discussed previously by Schimpf and co-workers in photodoped ZnO NCs.[10] Each hole that is quenched by sacrificial reductant results in the addition of an electron to NCs. After the successful addition of the first electron, further hole quenching must have to compete with the recombination involving photoexcited and already-added electrons. If photogenerated holes are recombined with excited electrons before they are transferred to a sacrificial reductant, no further electron addition will happen. This process is typically called trion recombination.[27] The hole quenching with sacrificial reductant must beat carrier recombination for the successive addition of electrons. We propose that relatively a few added electrons at the early stages of photodoping make the hole quenching reaction much more effective than recombination. Because the recombination rate increases with the number of added electrons, every successive addition of electrons makes recombination processes more competitive which slows down the rate of electron accumulation as the photodoping time progresses.[28]

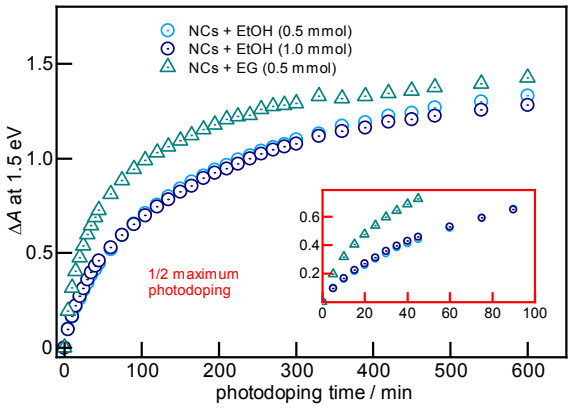

Fig. 2 The changes in absorbance at 1.5 eV ($\Delta A = A_{photodoped} - A_{as\text{-}prepared}$) as a function of photodoping time in the presence of two different concentrations of ethanol (0.5 and 1 mmol) and ethylene glycol. Inset: zoomed-in view showing the first 100 minutes of photodoping for both reductants.

The absorbance of the near-IR electronic transition at 1.5 eV is plotted versus photodoping time for two different sacrificial reductants in Fig. 2. For this set of experiments, we prepared a stock sample of $SrTiO_3$ NCs suspended in toluene and added either ethanol (EtOH) or ethylene glycol (EG). Both EtOH and EG were in large excess relative to the concentration of NCs. Under identical photodoping conditions, the kinetics of the near-IR absorbance for both reductants fit well to biexponential functions (see Fig. S5). The kinetics is relatively unaffected with doubling the concentration of EtOH (see Figs 2 and S3-S4).

However, the photodoping kinetics in the presence of EG has a faster rate of electron accumulation. The time it takes to reach 50% of the absorbance value after 10 h of photodoping is only ~50 min for EG compared to ~100 min with EtOH (see Figure 2 inset). It is also apparent that the near-IR absorption nearly approaches a steady-state value at long photodoping times in the presence of EG, while photodoping in the presence of EtOH does not yet reach steady-state even after 10 hours of irradiation.

Quantitative analysis of the kinetic parameters confirms faster rates and a significantly larger pre-exponential factor for the fast component of the photodoping process when EG is used instead of EtOH (see Table S1). Multiple groups have shown that the rate of H_2 evolution from aqueous suspensions on M/TiO_2 photocatalyst surfaces is very sensitive to the identity of the hole quenching alcohol with rates following the trend: triols > diols > 2° alcohols > 1° alcohols > 3° alcohols.[29,30] This established trend was found to correlate with numerous chemical properties of the alcohol including the number of α-H's, chemical polarity, polarizability, and oxidation potential of the alcohol.[29] For example, high polarity alcohols have been reported to interact strongly with the TiO_2 surface, while the number of α-H represents the active sites for their oxidation resulting in efficient electron transfer from the hole quencher to the TiO_2 valence band.[31] Similarly, the redox potential determines the driving force of the hole quencher: more negative redox potential leads to a faster hole quenching and vice versa. In fact, EG has been previously reported as a highly effective hole quencher to suppress the photoexcited charge recombination in TiO_2.[32] Therefore, we also propose that the more negative redox potential of EG (0.009 V) compared to EtOH (0.084 V), and other physical properties such as α-H's, polarity, and polarizability provide a reasonable explanation for the trend in photodoping kinetics shown in Fig. 2.

Despite a difference in rates, the photodoping with EtOH and EG eventually reaches a similar steady-state absorbance where further UV irradiation yields no significant spectroscopic changes. The typical photodoping process is not just governed by the successful addition of electrons but also coupled with the transfer of protons at the surfaces for charge compensation.[11] For instance, Valdez and co-workers have shown a linear relationship between the number of added electrons and protons per ZnO NC.[33] Each EtOH molecule donates two electrons and two protons upon its oxidation to acetaldehyde.[34] We also observed the characteristic quartet signal for the aldehydic proton of acetaldehyde in the ^{1}H-NMR spectra of photodoped samples at δ = 9.6 ppm (see Figs S6-S7). This indicates that electron addition in $SrTiO_3$ NCs is also gated by the adsorption of protons produced during EtOH oxidation to acetaldehyde. More importantly, the presence of these surface protons and acetaldehyde can play an important role in the saturation of photodoping over time. We speculate that the microscopic origin of such a steady-state at long photodoping times could be the hydrogenation of acetaldehyde to EtOH as observed in photodoped ZnO.[35] This reduction reaction is sensitive to changes in the Fermi level which at low electron densities is negligible but dominates with increased photodoping time.[35] Therefore, at the later stages of photodoping, EtOH oxidation is spontaneously equilibrated by the reduction of acetaldehyde, and no further electrons are added to $SrTiO_3$ NCs.

Although stable indefinitely under anaerobic conditions, these photodoped colloidal NCs can be reversed quantitatively by simply exposing the samples to air. This reversibility makes photodoped colloidal NCs amenable to direct titration with chemical oxidants to quantify the number of added electrons – something not practicable with chemically reduced bulk powders. We quantified the average number of electrons added per nanocrystal (⟨n⟩) by redox titration with the one-electron oxidant 2,2,6,6-tetramethylpiperidinyloxy (TEMPO) under a strictly anaerobic environment using a custom-made cuvette (see ESI). A detailed experimental procedure with various steps to estimate ⟨n⟩ is provided in the ESI (see Figs S8-S11 and Tables S2-S6).

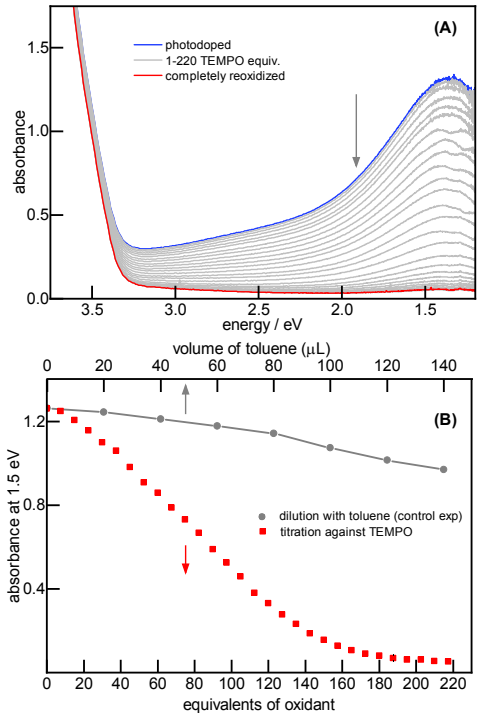

Fig. 3 **(A)** Electronic absorption spectra of photodoped NCs with the sequential addition of TEMPO. **(B)** The change in absorbance at 1.5 eV plotted against the equivalent of TEMPO. The error bars are shown in grey vertical capped lines and the top grey data shows the change in absorbance of photodoped NCs with the addition of toluene as a control experiment.

Fig. 3A shows the representative UV-Vis absorption spectra collected 2 min after adding each aliquot of TEMPO. The average changes in absorbance at 1.5 eV plotted against equivalents of oxidant are shown in Fig. 3B. These titration experiments were reproduced in triplicate using the same batch of photodoped NCs (see Figs S12-S13). The data shown above displays a gradual decay of the broad absorption feature associated with excess electrons upon the addition of TEMPO resulting in oxidized NCs. The mechanism of this redox titration has previously been studied which involves the transfer of an electron and a proton from photodoped NCs to TEMPO

radical.[11,36] With TEMPO being a one-electron oxidant, the complete elimination of absorbance at 1.5 eV provides an estimate of $\langle n \rangle$ = ~180 corresponding to a carrier concentration of $N = 5.3\times10^{20}$ cm^{-3} (see ESI for detailed calculations). This number for $SrTiO_3$ NCs reported here significantly exceeds the previous reports on sub-5 nm amorphous TiO_2 nanoparticles ($\langle n \rangle$ = 72), ZnO ($\langle n \rangle$ = 5), and CdSe ($\langle n \rangle$ = 2) NCs.[3,11] It is important to notice that excess electrons stored in the above-mentioned systems are typically delocalized in their conduction bands. However, excess electrons in $SrTiO_3$ NCs are localized at Ti^{3+} sites as discussed in the earlier section and in other reports.[37] The broad absorption feature at 1.5 eV that is assigned to IVCT transition in photodoped NCs suggests that Ti^{3+} trap states are situated well below the conduction band. This is the most distinctive feature of these photodoped $SrTiO_3$ NCs that allows large numbers of electrons to localize at Ti^{3+} sites.

The electron storage of photodoped $SrTiO_3$ NCs through self-trapping in deep Ti^{3+} sites make them promising materials for energy storage applications such as solution-processable redox-flow batteries and multielectron redox catalysis. We suspect that $\langle n \rangle$ will scale with the volume of the $SrTiO_3$ NCs similar to ZnO NCs.[10] Due to synthetic challenges in tuning the size of $SrTiO_3$ NCs while keeping the surface chemistry and morphology intact, the exploration of size dependence is currently underway. The electron storage density can also be further improved with the introduction of Fe^{3+} dopants which results in a stoichiometric increase in the number of electron trapping sites. We recently demonstrated a reversible electron addition at Fe^{3+} sites in colloidal Fe-doped $SrTiO_3$ NCs where the $Fe^{3+/2+}$ redox level is situated deeper than the $Ti^{4+/3+}$ redox level.[20] The experimental quantification of excess carriers in Fe-doped $SrTiO_3$ NCs as a function of Fe doping levels is currently underway.

This work was supported by the following awards from the U.S. National Science Foundation: DMR-1747593, CHE-1726578 (MRI for acquisition of XRD), and CHE-1659266 (to support RJN on REU). We thank Dr. Khushboo Singh for help with NMR measurements, and Sally Prasch for designing and fabricating the air-free glass apparatus for the redox titration experiments.

Notes and references

1. N. Seddon, *Science*, 2022, **376**, 1410-1416.
2. Y. Huang, M. Zhu, Y. Huang, Z. Pei, H. Li, Z. Wang, Q. Xue and C. Zhi, *Adv. Mater.*, 2016, **28**, 8344-8364.
3. J. D. Rinehart, A. M. Schimpf, A. L. Weaver, A. W. Cohn and D. R. Gamelin, *J. Am. Chem. Soc.*, 2013, **135**, 18782-18785.
4. A. M. Schimpf, S. D. Lounis, E. L. Runnerstrom, D. J. Milliron and D. R. Gamelin, *J. Am. Chem. Soc.*, 2015, **137**, 518-524.
5. F. Wu, H. Yang, Y. Bai and C. Wu, *J. Energy Chem.*, 2020, **51**, 416-417.
6. R. Chen, R. Luo, Y. Huang, F. Wu and L. Li, *Adv. Sci.*, 2016, **3**, 1600051.
7. A. Pannwitz and O. S. Wenger, *Chem. Commun.*, 2019, **55**, 4004-4014.
8. A. M. Schimpf, K. E. Knowles, G. M. Carroll and D. R. Gamelin, *Acc. Chem. Res.*, 2015, **48**, 1929-1937.
9. C. K. Brozek, D. Zhou, H. Liu, X. Li, K. R. Kittilstved and D. R. Gamelin, *Nano Lett.*, 2018, **18**, 3297-3302.
10. A. M. Schimpf, C. E. Gunthardt, J. D. Rinehart, J. M. Mayer and D. R. Gamelin, *J. Am. Chem. Soc.*, 2013, **135**, 16569-16577.
11. J. N. Schrauben, R. Hayoun, C. N. Valdez, M. Braten, L. Fridley and J. M. Mayer, *Science*, 2012, **336**, 1298-1301.
12. W. L. Harrigan and K. R. Kittilstved, *J. Phys. Chem. C*, 2018, **122**, 26652-26657.
13. W. K. Liu, K. M. Whitaker, K. R. Kittilstved and D. R. Gamelin, *J. Am. Chem. Soc.*, 2006, **128**, 3910-3911.
14. A. Janotti, J. B. Varley, M. Choi and C. G. van de Walle, *Phys Rev B*, 2014, **90**, 085202.
15. J.-i. Fujisawa, T. Eda and M. Hanaya, *Chem. Phys. Lett.*, 2017, **685**, 23-26.
16. W. L. Harrigan, S. E. Michaud, K. A. Lehuta and K. R. Kittilstved, *Chem. Mater.*, 2016, **28**, 430-433.
17. J. A. Noland, *Phys Rev*, 1954, **94**, 724-724.
18. D. Bahnemann, A. Henglein, J. Lilie and L. Spanhel, *J. Phys. Chem.*, 1984, **88**, 709-711.
19. D. Duonghong, J. Ramsden and M. Gratzel, *J. Am. Chem. Soc.*, 1982, **104**, 2977-2985.
20. M. Abdullah, R. J. Nelson and K. R. Kittilstved, *Chem. Mater.*, 2021, **33**, 4196-4203.
21. L. De Trizio, R. Buonsanti, A. M. Schimpf, A. Llordes, D. R. Gamelin, R. Simonutti and D. J. Milliron, *Chem. Mater.*, 2013, **25**, 3383-3390.
22. A. Yamakata, J. J. M. Vequizo and M. Kawaguchi, *J. Phys. Chem. C*, 2015, **119**, 1880-1885.
23. B. Bueken, F. Vermoortele, D. E. Vanpoucke, H. Reinsch, C. C. Tsou, P. Valvekens, T. De Baerdemaeker, R. Ameloot, C. E. Kirschhock, V. Van Speybroeck, J. M. Mayer and D. De Vos, *Angew. Chem. Int. Ed. Engl.*, 2015, **54**, 13912-13917.
24. G. Horrer, M. J. Krahfuß, K. Lubitz, I. Krummenacher, H. Braunschweig and U. Radius, *Eur. J. Inorg. Chem.*, 2020, **2020**, 281-291.
25. B. R. Mcgarvey, *J Chem Phys*, 1963, **38**, 388-392.
26. V. M. Khomenko, K. Langer, H. Rager and A. Fett, *Phys. Chem. Min.*, 1998, **25**, 338-346.
27. A. W. Cohn, A. M. Schimpf, C. E. Gunthardt and D. R. Gamelin, *Nano Lett.*, 2013, **13**, 1810-1815.
28. V. I. Klimov, A. A. Mikhailovsky, D. McBranch, C. A. Leatherdale and M. G. Bawendi, *Science*, 2000, **287**, 1011-1013.
29. Z. H. Al-Azri, W.-T. Chen, A. Chan, V. Jovic, T. Ina, H. Idriss and G. I. Waterhouse, *J. Catal.*, 2015, **329**, 355-367.
30. H. Bahruji, M. Bowker, P. R. Davies and F. Pedrono, *Appl. Cat. B: Environ.*, 2011, **107**, 205-209.
31. M. J. Berr, P. Wagner, S. Fischbach, A. Vaneski, J. Schneider, A. S. Susha, A. L. Rogach, F. Jäckel and J. Feldmann, *Appl. Phys. Lett.*, 2012, **100**, 223903.
32. N. Denisov, J. Yoo and P. Schmuki, *Electrochimica Acta*, 2019, **319**, 61-71.
33. C. N. Valdez, M. Braten, A. Soria, D. R. Gamelin and J. M. Mayer, *J. Am. Chem. Soc.*, 2013, **135**, 8492-8495.
34. K. Katsiev, G. Harrison, H. Alghamdi, Y. Alsalik, A. Wilson, G. Thornton and H. Idriss, *J. Phys. Chem. C*, 2017, **121**, 2940-2950.
35. G. M. Carroll, A. M. Schimpf, E. Y. Tsui and D. R. Gamelin, *J. Am. Chem. Soc.*, 2015, **137**, 11163-11169.
36. M. N. Braten, D. R. Gamelin and J. M. Mayer, *ACS Nano*, 2015, **9**, 10258-10267.
37. A. Yamakata, H. Yeilin, M. Kawaguchi, T. Hisatomi, J. Kubota, Y. Sakata and K. Domen, *J. Photochem. Photobio. A: Chem.*, 2015, **313**, 168-175.